1 **Sympathetic Transmitters Controlling Thermogenic Efficacy of Brown Adipocytes by**

2 **Modulating Mitochondrial Complex V**

3 **Running title: Thermogenic Efficacy of Brown Adipocytes**

4

5 **Tao-Rong Xie[*], Chun-Feng Liu[*], Jian-Sheng Kang[*#]**

6

7 CAS Key Laboratory of Nutrition and Metabolism, Institute for Nutritional Sciences, Shanghai

8 Institutes for Biological Sciences, Chinese Academy of Sciences; University of Chinese

9 Academy of Sciences, P. R. China.

10

11 * These authors contributed equally to this work.

12

13 Summary: 149; Characters: 21121

14 Number of references: 33; Number of figures: 4

15 Number Supplemental figures: 4

16 Number of Supplemental Movies: 5

17

18 # Correspondence should be addressed to J.-S. Kang, Institute for Nutritional Sciences,

19 Shanghai Institutes for Biological Sciences, Chinese Academy of Sciences, Building 34, Room

20 315, 294 Taiyuan Road, Shanghai 200031, China. Tel: 86-21-54920909; Fax: 86-21-54920961;

21 E-mail: jskang@gmail.com

22

Key words: mitochondrial thermometry; brown adipocyte; heterogeneity; thermogenesis; mitochondrial complex V; proton ATPase; ATP; sympathetic neurotransmitter; thermogenic efficacy

Highlights

1. Norepinephrine (NE) induces heterogeneous responses in brown adipocytes

2. NE activates the H^+-ATPase activity of mitochondrial complex V

3. Mitochondrial complex V is a key factor in NE-induced thermogenic efficacy

4. ATP as a sympathetic cotransmitter enhances the NE-induced thermogenic efficacy

ABSTRACT

Obesity is epidemic worldwide as the results of excessive energy intake or inefficient energy expenditure. It is promising to utilize the thermogenic function of brown adipose tissue for obesity intervention. However, the mechanisms controlling the efficacy of norepinephrine-induced thermogenesis in brown adipocytes remain elusive. Here, we demonstrate that the proton ATPase activity of mitochondrial complex V is a key factor, which antagonizes proton leak by UCP1 and determines the efficacy of norepinephrine-induced thermogenesis in brown adipocytes. Furthermore, to avoid unnecessary and undesired heat production, we reveal that ATP as a sympathetic cotransmitter is necessary for the high efficacy and specificity of norepinephrine-induced thermogenesis in brown adipocytes by upregulating the ATP synthase activity of complex V. Thus, we demonstrate the modulation mechanism of thermogenic efficacy in brown adipocytes. These findings imply new strategies for efficiently utilizing brown adipocytes thermogenic capacity, and therapeutic targets for the treatments of obesity and diabetes.

1 **INTRODUCTION**

2 Obesity is epidemic worldwide as the results of excessive energy intake or inefficient energy

3 expenditure. Brown adipose tissue (BAT) is the major tissue for cold-induced thermogenesis

4 (energy dissipation as heat) without shivering(1)'(2). Identification of functional BAT in adult

5 humans(3)'(4)'(5) suggests that it is promising to utilize BAT thermogenic capacity for obesity

6 and diabetes treatments(6)'(7).

7

8 Currently, the mechanism of thermogenesis in BAT and brown adipocytes (BA) is known in

9 general(2). Cutaneous thermosensory signals for cold stimulation evoke sympathetic nerve firing

10 in BAT via hypothalamus(8). Released neurotransmitter norepinephrine (NE) binds

11 adrenoreceptors of BA, upregulates hormone-sensitive lipase (HSL)-mediated lipolysis via

12 phosphorylation by protein kinase A (PKA) signaling, mobilizes free fatty acids to activate

13 mitochondrial uncoupling protein-1 (UCP1), and converts electrochemical potential energy

14 stored in mitochondrial proton gradient to heat(2)'(9). However, our previous study demonstrates

15 a low thermogenic efficacy of NE-induced thermogenesis in BA (10), which may partially

16 account for the failures of trials to utilize BAT thermogenic capacity for obesity

17 intervention(11)'(12). Therefore, the regulatory mechanism of thermogenesis in BA is still largely

18 unknown. In this study, we demonstrate that proton-ATPase function of mitochondrial complex V

19 accounts for NE-induced heterogeneous changes in BA and that sympathetic cotransmitter ATP

20 enhances the efficacy of thermogenesis in BA.

21

22

RESULTS

NE induces heterogeneous responses in BA

We consistently observe that NE induces heterogeneous changes of mitochondrial membrane potentials (MMP) in BA (Figure 1), which is monitored with thermoneutral rhodamine 800 (Rh800, a thermal-insensitive mitochondrial marker and MMP sensor)(17) (10). Obviously, there are two MMP populations (depolarization and hyperpolarization) of NE-induced thermogenesis in BA (Figure 1A-H), in line with previous studies (18) (10). The subpopulation of MMP depolarization can be explained by the activation of UCP1 dissipating electrochemical potential energy of proton as heat. The diverse extent of MMP depolarization evoked by NE may be explained by heterogeneity and different NE affinity of β adrenergic receptors(19) or the heterogeneous levels of UCP1 expression(20).

To test such explanation, we have checked the potential relationship between the heterogeneity of MMP changes and the extent of HSL phosphorylation at Ser563 (Figure S1), since HSL serves as a downstream lipase of β adrenergic receptors. After NE stimulation and monitoring the responses of MMP, we have retrospectively immunostained the BA with antibody against phospho-HSL and assumed that BA with high levels of phosphorylated HSL should correlate with mitochondrial depolarization. However, BA with high levels of phosphorylated HSL (arrows and red arrow head) either show mitochondrial depolarization (arrow heads) or hyperpolarization (arrows), while BA with low levels of phosphorylated HSL (white arrow heads) can show mitochondrial depolarization (Figure S1B,C and F). Secondly, treatments with NE concentration raised 100 fold to 10 μM still show two MMP populations (Figure 1G). These

1   results suggest that the heterogeneous changes of MMP are unlikely correlated to the

2   heterogeneity of adrenoreceptors or different activity of HSL. In addition, we have also found

3   that all BA express UCP1 although at heterogeneous levels (Figure S2A-D), and that

4   mitochondrial hyperpolarization is not due to the absence of UCP1 (Figure S2E-G). The different

5   activity of HSL and heterogeneity of UCP1 may account for the diverse extent of MMP

6   depolarization.

7

Correlations among NE-induced heterogeneous responses in BA

9   With the thermosensitive Rhodamine B methyl ester (RhB-ME) based mito-thermotry (Xie et al.,

10   2017), we observe that the NE-induced thermogenic responses (the fluorescent intensity ratio of

11   Rh800 to RhB-ME) in BA indeed show negative correlation with mitochondrial electric potential

12   difference ($\Delta\Psi_m$) (Figure 1D-F and movie 1-2). Our findings suggest that the heterogeneous

13   responses of MMP in BA can index NE-induced thermogenic efficacy, and further confirm that

14   the efficacy of NE-induced thermogenesis is low (10). Especially, even high concentration (10

15   μM) of NE still shows low efficacy with two $\Delta\Psi_m$ populations (Figure 1G) and only slightly

16   increases thermogenic responses of BA compared to the stimulation of 0.1 μM NE (Figure 1H).

17   Meanwhile, NE-induced thermogenic responses of BA are inhibited by 1 μM SR-59230A (a

18   potent β adrenergic receptors antagonist, Figure 1H).

19

20   Considering mitochondrial $\Delta\Psi_m$ is quasi-linear in physiologically relevant ranges of the pH

21   difference (ΔpH)(21), MMP hyperpolarization might result from cytoplasmic acidification by

22   enhanced glycolysis or NE-stimulated activities of proton pumps. Indeed, using SNARF1-AM, a

1   ratiometric pH-indicating fluorescent probe, we reveal that the subpopulation of MMP

2   hyperpolarization shows cytoplasmic acidification (ΔpH < 0), and $\Delta\Psi_m$ shows negatively

3   correlated with ΔpH (Figure 1I).

4

5   Intriguingly, the correlations among NE-induced thermogenic responses, $\Delta\Psi_m$ and ΔpH

6   give us a hint that mitochondrial thermogenesis of BA might be the net result of proton outflow by

7   pumps and proton leak by UCP1.

8

9   **NE stimulation activates the proton ATPase activity of mitochondrial complex V in BA**

10   Cytoplasmic acidification of MMP hyperpolarized BA (Figure 1I) can be not only explained by

11   NE-acitivated proton ATPase (H^+-ATPase) but also by enhanced glycolysis. To distinguish the

12   difference and potential roles of the enhanced glycolysis (net ATP production) or NE-activated

13   mitochondrial H^+-ATPase (ATP consumption) in BA, we next examine the statuses of

14   mitochondrial and cytoplasmic ATP concentration ([ATP]) after NE stimulation (Figure 2A-G).

15   With FRET-based ATP indicators (mitAT1.03 and AT1.03)(22), we find that both of cytoplasmic

16   [ATP] and majority of mitochondrial [ATP] are decreased (Figure 2C and E) after NE stimulation

17   of BA.

18

19   Clearly, these results suggest that NE stimulation activates an ATPase, which is likely a

20   H^+-ATPase and might play a role in the thermogenic efficacy of BA. The best candidate for

21   H^+-ATPase is mitochondrial ATP synthase/complex V, which can function as an ATPase to

22   pump protons out of mitochondrial matrixes(23). ATP is not only consumed by mitochondrial

1   ATPase but also other cellular activities. Therefore, it is necessary to further check whether

2   complex V is the ATPase activated by NE. Thus, we use oligomycin A, a specific inhibitor of

3   complex V, and reveal that oligomycin A mitigates ATP consumption induced by NE stimulation

4   (Figure 2F and G). These results confirm that NE activates the ATPase function of mitochondrial

5   complex V.

6

7   The role of mitochondrial complex V as ATPase is quite provocative. For example, where

8   does ATP come from? The source of ATP production can be provided by NE-stimulated

9   metabolism of glucose, since it has been reported and well known that glucose uptake is

10   increased in BA or BAT by one or two orders of magnitude in human (12 folds) and rat (110

11   times) under cold stimulation(24),(25). NE-stimulated metabolism in BA is indeed supported by

12   accelerated-metabolic status represented with homogenous redox changes (Figure S3A-H),

13   which are endogenous autofluorescences and ratio measurement of FAD and NADH (16). In

14   addition, interestingly illustrated in Figure 2F, a few of BA pretreated with oligomycin A show

15   transiently increased cytoplasmic [ATP], which support accelerated cytosol metabolism for ATP

16   production after NE stimulation.

17

18   In addition, to further check whether the ATPase function of complex V causes cytoplasmic

19   acidification after NE stimulation, we use oligomycin A to inhibit complex V again and reveal that

20   almost all of BA show cytoplasmic alkalizations ($\Delta pH > 0$) and that majority of BA show MMP

21   depolarization after NE stimulation (Figure 2H). Thus, these findings further demonstrate and

22   confirm that NE stimulation activates the H^+-ATPase function of complex V rather than glycolysis

1   for cytoplasmic acidification. Together, our findings suggest that the H^+-ATPase activity of

2   complex V is a key factor to antagonize proton leak by UCP1, impact on the net cytoplasmic

3   ΔpH (Figure 1I and Figure 2H) and modulate the efficacy of NE-induced BA thermogenesis.

4

5   **ATP as a sympathetic cotransmitter can increase the NE-induced thermogenic efficacy**

6   Our observations suggest that more factors other than NE alone are needed for the high efficacy

7   of evoking thermogenesis in BAT. Considering ATP is also a neurotransmitter and co-released

8   with NE when sympathetic nerve firing is evoked(26), we examine whether ATP is a co-factor

9   needed for NE to efficiently evoke thermogenesis of BA (Figure 3). As illustrated in Figure 3,

.0   majority of BA show thermogenic responses (Figure 3A-C) to NE and ATP co-stimulation (movie

.1   3-4). The co-treatment with NE and ATP also increases the percentage (in mean ± SD) of MMP

.2   depolarization subpopulation (72.8% ± 13.3%) in BA compared to NE treatment alone (55.6% ±

.3   16.1%, P = 0.0514, one sided t-test) (Figure 3D-E). NE and ATP co-stimulation markedly

.4   increases the amplitudes of thermogenic responses (Figure 3F) in BA compared to NE

.5   treatment alone (Movie 1-4). Whereas, BA only show slightly and relative flat responses to ATP

.6   treatment alone (Figure 3F).

.7

.8   To elucidate the enhancement effect of sympathetic cotransmitter ATP via purinergic

.9   receptors, we check the statuses of cytoplasmic and mitochondrial Ca^{2+} concentration ($[Ca^{2+}]$)

!0   with ratiometric probe Fura2-AM and indicator 4mtD3cpv(27) respectively (Figure 4 and S4). We

!1   find that extracellular ATP evokes transient elevation of cytoplasmic $[Ca^{2+}]$ (Figure 4A and C) in

!2   BA through multiple P2 receptors (Figure S4 and Movie 3) in line with previous reports(28).

1   Whereas, we find that extracellular ATP evokes transient peaked and steady elevation of

2   mitochondrial $[Ca^{2+}]$ (Figure 4B and D), which can upregulate mitochondrial oxidative

3   phosphorylation(29).

4

5   Therefore, we examine the states of cytoplasmic and mitochondrial [ATP] after ATP

6   stimulation (Figure 4E-H). We observe a steady elevation of mitochondrial [ATP] while no

7   apparent change of cytoplasmic [ATP] after extracellular ATP stimulation (Figure 4E-H). These

8   findings suggest that sympathetic co-transmitter ATP increases the ATP synthase activity of

9   complex V for ATP production (Figure 4H) by elevating mitochondrial $[Ca^{2+}]$ (Figure 4D).

10   Importantly, the thermogenic enhancing function (Figure 3) of ATP as sympathetic co-transmitter

11   of NE can explain the discrepancy of cold and sympathomimetics activities on human BAT *in*

12   *vivo*(30).

13

14

15   **DISCUSSION**

16   **Mitochondrial complex V is a deterministic factor in NE-induced thermogenic efficacy**

17   How does the H^+-ATPase activity of complex V modulate the thermogenic efficacy of BA? A first

18   straightforward explanation is endothermic characteristic feature of ATP hydrolysis by

19   mitochondrial complex V(31), which pumps dissipated proton back and restore energy in

20   mitochondrial proton gradient. In Figure 1E, there are some interesting and supporting results,

21   where very a few BA show endothermic profiles rather than exothermic profiles to NE stimulation.

22   The endothermic profiles could be a stimulus artifact but unlikely. Secondly, H^+-ATPase activity

1   of complex V results in cytoplasmic acidification (Figure 1I and Figure 2H), which can enhance

2   the binding and inhibition of purine nucleotides to UCP1(32).

3

4   Why need the function of complex V as H^+-ATPase by NE stimulation? The physiological

5   role of the H^+-ATPase function is likely to avoid unnecessary and undesired heat production

6   since NE is either secreted by adrenal medullae or released by sympathetic nervous system,

7   which can be also excited by mental or physical stress (33). Accordingly, for cold stimulation, our

8   observations suggest that at least two factors (NE and ATP) are needed for the high efficacy and

9   specificity of evoking thermogenesis in BAT.

.0

.1   In this study, we have observed that NE evokes both homogenous responses (of redox

.2   ratio, cytosol ATP consumption and calcium dynamics) and heterogeneous changes (in MMP,

.3   cytosol pH and thermogenesis). Consequently, we have demonstrated that the heterogeneous

.4   changes and thermogenic efficacy are modulated by the functional status of mitochondrial

.5   complex V. Our findings suggest that mitochondrial malfunctions or impairments in sympathetic

.6   system or BAT can be pathologic reasons for inefficient energy expenditure and developing

.7   obesity. Additionally, our current observations also open new doors and pave ways to reconsider

.8   targets and strategies of fully utilizing brown adipocytes thermogenic capacity for the treatments

.9   of obesity, diabetes and abnormal lipid metabolism.

!0

!1   **MATERIALS and METHODS**

!2   Data are pooled from or repeated for each condition at least three independent

1 experiments. No statistical methods were used to predetermine sample size. All data points in

2 figures represent mean ± SEM except Figure 3E, which data in text or figures represent mean ±

3 SD. More detailed information of the Experimental Procedures can be found in the Supplemental

4 Data.

5

6 Isolation and primary culture of brown adipocytes

7 Brown adipocytes (BA) were isolated from 3-4weeks male C57BL/6J mice, with a

8 procedure similar to that described by Lucero *et al.* (13). Briefly, mice were kept at 4 °C for

9 overnight with free access to food and water to deplete stored lipid in brown adipose tissues

10 (BAT). The mice were then sacrificed by cervical dislocation and swabbed with 75% ethanol.

11 Interscapular BAT was isolated and placed in isolation buffer (DMEM with 4% NCS). The tissue

12 was minced and digested with 0.2% collagenase type II in a shaking water bath at 37 °C for 30

13 min (14). After digesting, discarded the reaction mixture, and the tissue was washed with

14 isolation buffer. Dissociated cells by gently triturating with fire-polish pipettes and washed by

15 centrifugation in PBS. After the final washing, the cells were plated onto 12 mm coverslips

16 ($\sim 3 \times 10^4$ cells per coverslip). Coverslips were precoated with matrigel. After 2 hours, 2 ml plating

17 medium (DMEM supplemented with 5% FBS, 100 units/ml penicillin and 100 μg/ml streptomycin)

18 was added to each 35 mm dish. From the second day in culture, half of the medium was

19 replaced with feeding medium (plating medium supplemented with Ara-C to inhibit fibroblast

20 proliferation, 2 μM final concentration of Ara-C) every 2 days. Cells were maintained at 37 °C in

21 a humidified atmosphere of 95% air and 5% CO_2, and used for imaging at 3~8 days *in vitro*.

22

Cell transfection

BA were washed with PBS and resuspended in electroporation solution (20 mM Hepes, 135 mM KCl, 2 mM MgCl$_2$, 0.5% Ficoll 400, 1% DMSO, 2 mM ATP and 5 mM glutathione, pH 7.6) with 20 µg of plasmid DNA (15). Two pulses (115 V, 10 ms duration) with 1s interval were delivered to electroporate cells (1-1.5×10^6 cells/ml) with an ECM 830 Square Wave Electroporation System (Harvard Apparatus, Inc., USA). Then, cells were seeded onto matrigel-coated coverslips. BA were maintained in DMEM supplemented with 5% FBS until imaging.

Thermogenic study

All imagings were performed using confocal microscope with a 40×/0.95 objective (Olympus) for time-lapse imaging and a 100×/1.4O objective (Olympus) for high-resolution imaging (Xie et al., 2017). Cells were co-stained with RhB-ME and Rh800 (20 nM dyes for time-lapse imaging, 50 nM dyes for high resolution imaging) in Tyrode's solution (in mM: 10 Hepes, 10 glucose, 3 KCl, 145 NaCl, 1.2 CaCl$_2$, 1.2 MgCl$_2$, pH 7.4) for 1 h at 33 °C. The pseudocolor of RhB-ME channel is red (excited at 559 nm and collected at 575-620 nm), and Rh800 channel is green (excited at 635 nm and collected at 655-755 nm). All images were collected at 512 × 512 (for time-lapse imaging) and 1600 ×1600 (for high resolution imaging) pixels resolution (12 bit). All data analysis was performed with MATLAB (MathWorks Inc. USA) or ImageJ (NIH, USA).

Cytoplasmic pH study

Cytoplasmic pH imagings were performed using confocal microscope with a 40×/0.95 objective (Olympus) for time-lapse imaging. Cells were co-stained with 5µM SNARF1-AM and 20 nM Rh800 in Tyrode's solution for 30 min at 37 °C. Then wash out SNARF1-AM using Tyrode's solution (with 20 nM Rh800). The pseudo color of acidification channel is red (excited by 561 nm laser and collected with 575-600 nm band pass filter), and alkalization channel is green (simultaneously collected with 600-675 nm band pass filter); Rh800 channel is magenta (sequentially excited by 635 nm laser and collected with 655-755 nm band pass filter). Ratiometric values of acidification channel to alkalization channel were calculated pixel by pixel to represent the relative pH value of the sample. The other conditions of imaging, data acquisition and analysis for cytoplasmic pH study were the same as the conditions in thermogenic study.

Redox (FAD/FAD+NADH) measurement

Redox (FAD/FAD+NADH) imagings were performed using a customized fluorescence microscope with a 40×/0.8W objective (Olympus) for time-lapse imaging. The endogenous autofluorescence images(16) were excited with Optoscan monochromator (Cairn Research Ltd., UK). The pseudocolor of FAD channel is red (excited by 430 nm light with 20 nm bandwith and collected with 525-575 nm band pass filter), while NADH+FAD channel is green (sequentially excited by 340 nm light with 20 nm bandwith and collected with 420 nm long pass filter). And the fluorescence images were acquired with Evolve 512 EMCCD (Photometrics Ltd., UK).

Time-lapse imagings of BA were performed in 4 mL Tyrode's solution at 33 °C. 60 frames were recorded in a time-lapse imaging at 30 seconds interval. NE (0.1 µM) was injected as soon as

1   the 11th frame of the time-lapse imaging for Redox studies in BA. The other conditions of

2   imaging, data acquisition and analysis for Redox study were the same as the conditions in

3   thermogenic study.

4

5   **Cytoplasmic [Ca^{2+}] study**

6   Cytoplasmic [Ca^{2+}] imagings were performed using the customized fluorescence

7   microscope with a 40×/0.8W objective (Olympus) for time-lapse imaging and Optoscan

8   monochromator (Cairn Research Ltd., UK) as light source. Cells were stained with 5μM

9   Fura2-AM in Tyrode's solution for 30 min at 37 °C. Then wash out Fura2-AM using Tyrode's

10   solution. The pseudocolor of 380 nm channel is red (excited by 380 nm light with 10 nm

11   bandwith and collected with 505-535 nm band pass filter), and 340 nm channel is green

12   (sequentially excited by 340 nm light with 10 nm bandwith and also collected with 505-535 nm

13   band pass filter). Ratiometric values of 340 nm channel to 380 nm channel were calculated pixel

14   by pixel to represent the relative [Ca^{2+}] of the sample. The other conditions of imaging, data

15   acquisition and analysis for cytoplasmic [Ca^{2+}] study were the same as the conditions in Redox

16   study.

17

18   **Mitochondrial [Ca^{2+}] study**

19   Mitochondrial [Ca^{2+}] imagings were performed using confocal microscope with a 40×/0.95

20   objective (Olympus) for time-lapse imaging. Cells were transfected with 4mtD3cpv (from Dr. R.

21   Tsien) using ECM 830 Square Wave Electroporation System (Harvard Apparatus, Inc., USA).

22   The pseudocolor of CFP channel is cyan (excited by 440 nm laser and collected with 480-495

1   nm band filter), and YFP channel is magenta (simultaneously collected with 505-605 nm band

2   filter). Ratiometric values of YFP channel to CFP channel were calculated pixel by pixel to

3   represent the relative [Ca^{2+}] of the sample. The other conditions of imaging, data acquisition and

4   analysis for mitochondrial [Ca^{2+}] study were the same as the conditions in cytoplasmic [Ca^{2+}]

5   study.

6

7   **Cytoplasmic and mitochondrial [ATP] study**

8   [ATP] imagings were performed using confocal microscope with a 40×/0.95 objective

9   (Olympus) for time-lapse imaging. Cells were transfected with AT1.03 for cytoplasmic [ATP] or

10   mitAT1.03 for mitochondrial [ATP] (from Dr. H. Noji and Dr. H. Imamura) using ECM 830 Square

11   Wave Electroporation System (Harvard Apparatus, Inc., USA). The pseudocolor of CFP channel

12   is cyan (excited at 440 nm and collected at 480-495 nm), and YFP channel is magenta

13   (simultaneously excited at 440 nm and collected at 505-605 nm). Ratiometric values of YFP

14   channel to CFP channel were calculated pixel by pixel to represent the relative [ATP] of the

15   sample. The other conditions of imaging, data acquisition and analysis for [ATP] study were the

16   same as the conditions in thermogenic study.

17

18   **Supplemental Data**

19   Supplemental Data include Supplemental four figures and five movies.

20

21   **Author Contributions** T.R.X. and C.F.L. designed and conducted the experiments and

22   manuscript writing. T.R.X. did live cell imaging and data analysis. C.F.L. did primary cell culture

and imaging. J.S.K. built the custom microscopy, developed the idea, directed the study and

wrote the paper. All authors participated in discussions.

Competing financial interests

The authors declare no competing financial interests.

REFERENCES

1. Lowell BB, Spiegelman BM (2000) Towards a molecular understanding of adaptive thermogenesis. *Nature* 404(6778):652–660.

2. Cannon B, Nedergaard J (2004) Brown Adipose Tissue: Function and Physiological Significance. *Physiol Rev* 84(1):277–359.

3. Cypess AM, et al. (2009) Identification and Importance of Brown Adipose Tissue in Adult Humans. *N Engl J Med* 360(15):1509–1517.

4. van Marken Lichtenbelt WD, et al. (2009) Cold-Activated Brown Adipose Tissue in Healthy Men. *N Engl J Med* 360(15):1500–1508.

5. Virtanen KA, et al. (2009) Functional Brown Adipose Tissue in Healthy Adults. *N Engl J Med* 360(15):1518–1525.

6. Harms M, Seale P (2013) Brown and beige fat: development, function and therapeutic potential. *Nat Med* 19(10):1252–1263.

7. Betz MJ, Enerbäck S (2015) Human Brown Adipose Tissue: What We Have Learned So Far. *Diabetes* 64(7):2352–2360.

8. Nakamura K, Morrison SF (2008) A thermosensory pathway that controls body temperature. *Nat Neurosci* 11(1):62–71.

9. Fedorenko A, Lishko PV, Kirichok Y (2012) Mechanism of Fatty-Acid-Dependent UCP1 Uncoupling in Brown Fat Mitochondria. *Cell* 151(2):400–413.

10. Xie T-R, Liu C-F, Kang J-S (2017) Dye-based mito-thermometry and its application in thermogenesis of brown adipocytes. *Biophys Rep*. doi:10.1007/s41048-017-0039-6.

11. Arch JRS (2011) Challenges in β3-adrenoceptor agonist drug development. *Ther Adv Endocrinol Metab* 2(2):59–64.

12. Carey AL, et al. (2012) Ephedrine activates brown adipose tissue in lean but not obese humans. *Diabetologia* 56(1):147–155.

13. Lucero MT, Pappone PA (1989) Voltage-gated potassium channels in brown fat cells. *J Gen Physiol* 93(3):451–472.

14. Fain JN, Reed N, Saperstein R (1967) The Isolation and Metabolism of Brown Fat Cells. *J Biol Chem* 242(8):1887–1894.

15. Burchfield JG, Lopez JA, Hughes WE (2012) Using Total Internal Reflection Fluorescence Microscopy (TIRFM) to Visualise Insulin Action. *Visualization Techniques*, Neuromethods., ed Badoer E (Humana Press), pp 97–109.

16. Georgakoudi I, Quinn KP (2012) Optical Imaging Using Endogenous Contrast to Assess Metabolic State. *Annu Rev Biomed Eng* 14(1):351–367.

17. Sakanoue J, Ichikawa K, Nomura Y, Tamura M (1997) Rhodamine 800 as a Probe of Energization of Cells and Tissues in the Near-Infrared Region: A Study with Isolated Rat Liver Mitochondria and Hepatocytes. *J Biochem (Tokyo)* 121(1):29–37.

18. Wikstrom JD, et al. (2014) Hormone-induced mitochondrial fission is utilized by brown adipocytes as an amplification pathway for energy expenditure. *EMBO J* 33(5):418–436.

19. Lafontan M, Berlan M (1993) Fat cell adrenergic receptors and the control of white and brown fat cell function. *J Lipid Res* 34(7):1057–1091.

20. Cinti S, et al. (2002) CL316,243 and Cold Stress Induce Heterogeneous Expression of UCP1 mRNA and Protein in Rodent Brown Adipocytes. *J Histochem Cytochem* 50(1):21–31.

21. Schuster S, Ouhabi R, Rigoulet M, Mazat J-P (1998) Modelling the interrelation between the transmembrane potential and pH difference across membranes with electrogenic proton transport upon build-up of the proton-motive force. *Bioelectrochem Bioenerg* 45(2):181–192.

22. Imamura H, et al. (2009) Visualization of ATP levels inside single living cells with fluorescence resonance energy transfer-based genetically encoded indicators. *Proc Natl Acad Sci* 106(37):15651–15656.

23. Nicholls D, Fergusion S (2002) *Bioenergetics, 3rd Edition* (Academic Press). 3rd Ed. Available at: http://store.elsevier.com/Bioenergetics/David-Nicholls/isbn-9780080527932/ [Accessed October 26, 2016].

24. Orava J, et al. (2011) Different Metabolic Responses of Human Brown Adipose Tissue to Activation by Cold and Insulin. *Cell Metab* 14(2):272–279.

25. Vallerand AL, Perusse F, Bukowiecki LJ (1990) Stimulatory effects of cold exposure and cold acclimation on glucose uptake in rat peripheral tissues. *Am J Physiol - Regul Integr Comp Physiol* 259(5):R1043–R1049.

26. Burnstock G (2006) Historical review: ATP as a neurotransmitter. *Trends Pharmacol Sci* 27(3):166–176.

27. Palmer AE, Tsien RY (2006) Measuring calcium signaling using genetically targetable fluorescent indicators. *Nat Protoc* 1(3):1057–1065.

28. Omatsu-Kanbe M, Isono T, Matsuura H (2002) Multiple P2 receptors contribute to a transient increase in intracellular Ca2+ concentration in ATP-stimulated rat brown adipocytes. *Exp Physiol* 87(06):643–652.

29. Tarasov AI, Griffiths EJ, Rutter GA (2012) Regulation of ATP production by mitochondrial Ca2+. *Cell Calcium* 52(1):28–35.

30. Cypess AM, et al. (2012) Cold but not sympathomimetics activates human brown adipose tissue in vivo. *Proc Natl Acad Sci* 109(25):10001–10005.

31. Dittrich M, Hayashi S, Schulten K (2003) On the Mechanism of ATP Hydrolysis in F1-ATPase. *Biophys J* 85(4):2253–2266.

32. Rafael J, Pampel I, Wang X (1994) Effect of pH and MgCl2 on the binding of purine nucleotides to the uncoupling protein in membrane particles from brown fat mitochondria. *Eur J Biochem* 223(3):971–980.

33. Guyton A, Hall J (2006) *Textbook of Medical Physiology* (Elsevier Saunders, Philadelphia). 11th Ed. Available at: http://www.us.elsevierhealth.com/physiology/textbook-of-medical-physiology-hardcover/9780721602400/ [Accessed February 22, 2016].

1   **Figure legends**

2

3   **Figure 1. NE induces heterogeneous responses in BA.** (**A-F**), NE-induced thermogenic

4   responses in BA show negative correlation with $\Delta\Psi_{m.}$ (**A**), Representative MMP image of BA

5   after 0.1 µM NE treatment. Arrowheads point to BA with mitochondrial depolarization, while

6   arrows point to BA with mitochondrial hyperpolarization. Scale bar, 20 µm. (**B**), The

7   corresponding thermal image (ratio of Rh800 intensity to RhB-ME intensity) after 0.1 µM NE

8   treatment. The result shows that the low efficacy of NE-induced thermogenic responses in BA.

9   Some BA show thermogenic responses to NE (arrow heads), while some have no responses to

10   NE stimulation (arrows). (**C**), Differential interference contrast (DIC) image of BA. (**D**) The raw

11   data plots of MMP show subpopulations of depolarization and hyperpolarization in 0.1 µM NE

12   treated BA. Each colored trace represents mitochondrial membrane potential (MMP) change of

13   single BA (n = 150). (**E**) NE-induced thermal responses in BA. Each colored trace represents a

14   thermogenic response of single BA (n = 150). (**F**) The scatter plot of thermogenic responses (**D**)

15   versus MMP changes (**E**) induced by NE, which shows a negative correlation (r = -0.73, n = 150,

16   P = 2.97e-26, by Pearson's correlation coefficient test). The box plots of the depolarization

17   subpopulation and the hyperpolarization subpopulation show significantly different amplitudes of

18   thermogenic responses ($P = 1.88\times10^{-27}$, two sided t-test). (**G**) The raw data plots of MMP still

19   show two-subpopulations in 10 µM NE treated BA. Each colored trace represents a MMP

20   change of single BA (n = 102). (**H**) Thermogenic responses in BA are evoked by 0.1 µM NE

21   (black line, n = 150) and 10 µM NE (red line, n = 88) respectively. The blue line shows that

22   NE-induced thermogenic response of BA is inhibited by 1 µM SR-59230A (n = 97). All data

points in figures represent mean ± SEM. (**I**) A representative scatter plot of pH changes versus

MMP changes induced by 0.1 µM NE, which shows a linear and negative correlation (red line, r

= -0.67, n = 75, P = 3.94x10^{-11}, by Pearson's correlation coefficient test).

Figure 2. NE stimulates proton-ATPase activity of mitochondrial complex V in BA. (**A-G**)

Fluorescence of AT1.03 based ratiometric measurements of mitochondrial and cytoplasmic ATP.

(**A** and **B**), show fluorescence images of mitAT1.03 and AT1.03 transfected BA before and after

0.1 µM NE treatment respectively. Scale bar, 20 µm. (**C** and **D**), show raw data plots (**C**) and

average plot (**D**) of mitochondrial ATP change (n = 16) in 0.1 µM NE treated BA. Each colored

trace represents ATP change of single BA (**C**). (**E**), shows the raw data plots of cytoplasmic ATP

(n = 29) after NE treatment. Each colored trace represents ATP change of single BA. (**F**), shows

the raw data plots of cytoplasmic ATP (n = 23) after co-treatment of NE and oligomycin A. Each

colored trace represents ATP change of single BA. **(G)**, compares the averaged changes of

cytoplasmic ATP after the treatment of NE (n = 29) or the co-treatment of NE and oligomycin A

(n = 23), which show that the inhibitor (oligomycin A) of mitochondrial complex V mitigates ATP

consumption induced by NE stimulation. **(H)**, shows representative scatter plot of pH changes

versus MMP changes induced by 0.1 µM NE with (red, n = 75) or without (black, n = 75) 10

µg/mL oligomycin A pretreatment, which demonstrates that the inhibitor of mitochondrial

complex V blocks the activity of proton pump. All data points in **D** and **G** represent mean ± SEM.

Figure 3. Sympathetic cotransmitter ATP enhances NE-induced thermogenic efficacy in BA. (A and **B),** Representative thermal images of BA before and after 0.1 µM NE and 10 µM ATP co-treatment respectively. Scale bar, 20 µm. **(C),** 0.1 µM NE and 10 µM ATP induced thermal responses in BA. Each colored trace represents a thermogenic response of single BA (n = 158). **(D),** The dynamic plots of MMP demonstrate that majority of BA show MMP depolarization after NE and ATP co-treatment. Each colored trace represents a MMP dynamic of single BA (n = 158). **(E),** shows scatter plots of MMP depolarization percentage in 0.1 µM NE without (black) or with (red) ATP treated experiments. NE and ATP co-treatment increases the percentage of MMP depolarization (72.8% ± 13.3%) compared to NE treatment alone (55.6% ± 16.1%). Error bars in figure represent mean ± SD. **(F),** 0.1 µM NE without (black line, also in Fig. 1H) or with 10 µM ATP (red line, n = 158) induced thermogenesis in BA. The blue line shows the control results of ATP treatment alone in BA (n = 67). All data points in **F** represent mean ± SEM.

Figure 4. Sympathetic cotransmitter ATP enhances NE-induced thermogenic efficacy in BA through modulating the function of mitochondrial complex V. (**A-D),** Sympathetic cotransmitter ATP increases cytoplasmic and mitochondrial $[Ca^{2+}]$ in BA, which are both fluorescence-based ratiometric measurements. Scale bars, 20 µm. **(A),** shows fluorescence images (excited by 380 nm or 340 nm laser) of Fura2-AM stained BA before and after 10 µM ATP treatment respectively, and their positions in panel **C** are labeled with 1, 2 and 3 respectively. **(B),** shows fluorescence images of 4mtD3cpv transfected BA before and after 10 µM ATP treatment respectively, and their positions in panel **D** are labeled with 1, 2 and 3

1   respectively. (**C** and **D),** show that ATP induces cytoplasmic (n = 63) and mitochondrial (n = 14)

2   [Ca^{2+}] transient in BA respectively. (**E-H),** Fluorescence of AT1.03 based ratiometric

3   measurements of cytoplasmic and mitochondrial ATP concentration induced by extracellular

4   ATP. (**E** and **F),** show fluorescence images of AT1.03 and mitAT1.03 transfected BA before and

5   after 10 μM ATP treatment respectively. Scale bars, 20 μm. (**G** and **H)** show the averaged

6   change of cytoplasmic (n = 28) and mitochondrial (n = 31) ATP by 10 μM ATP treatment. All data

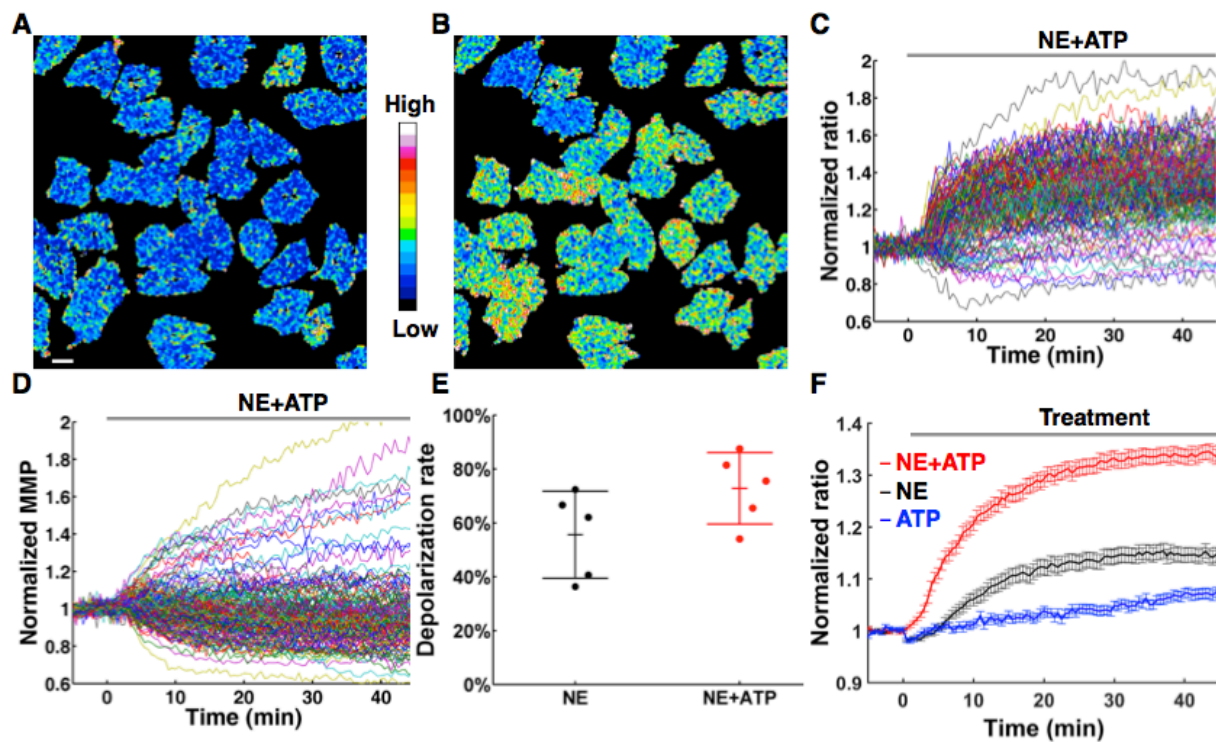7   points in **C**, **D**, **G** and **H** represent mean ± SEM.
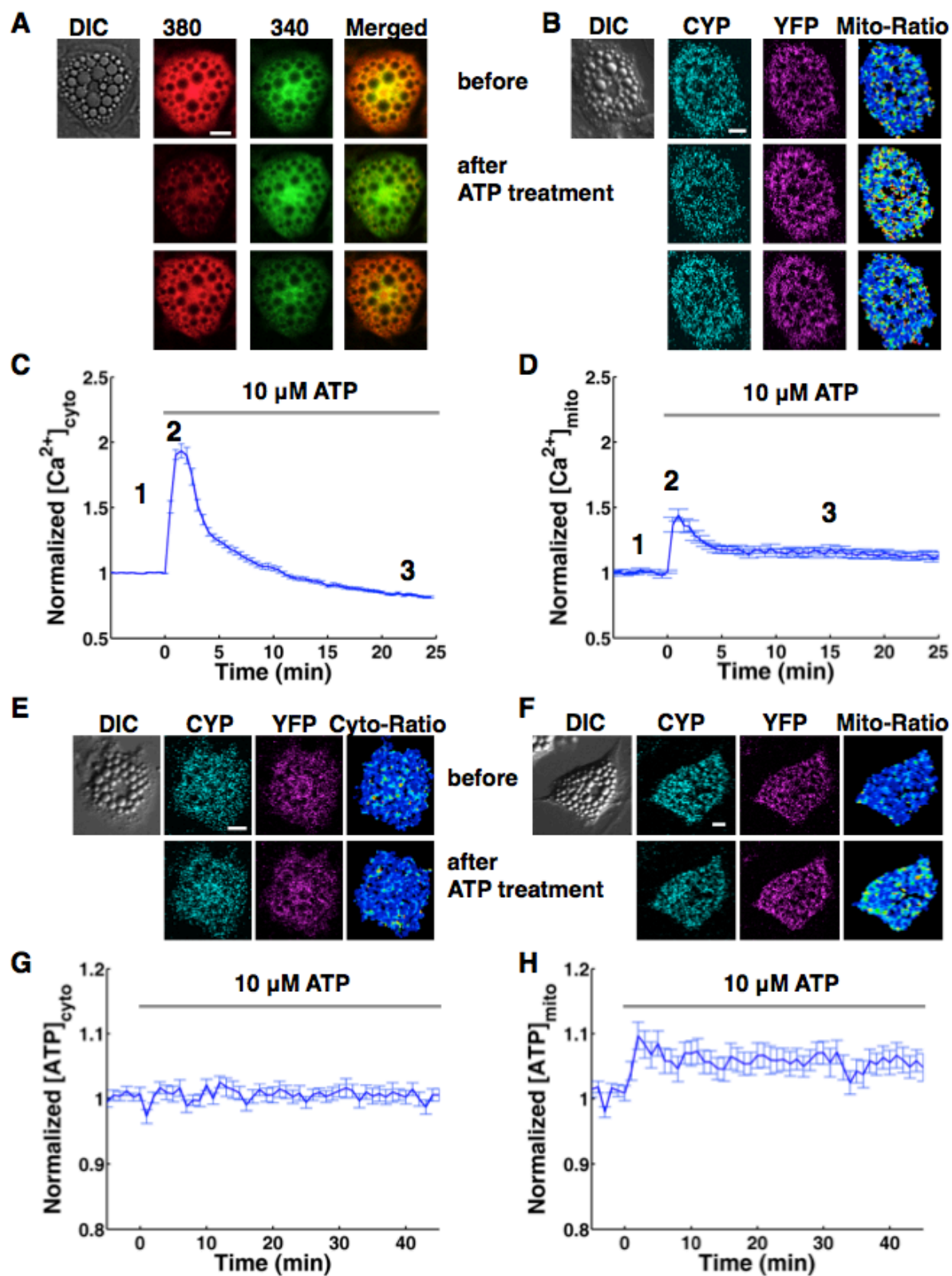
8
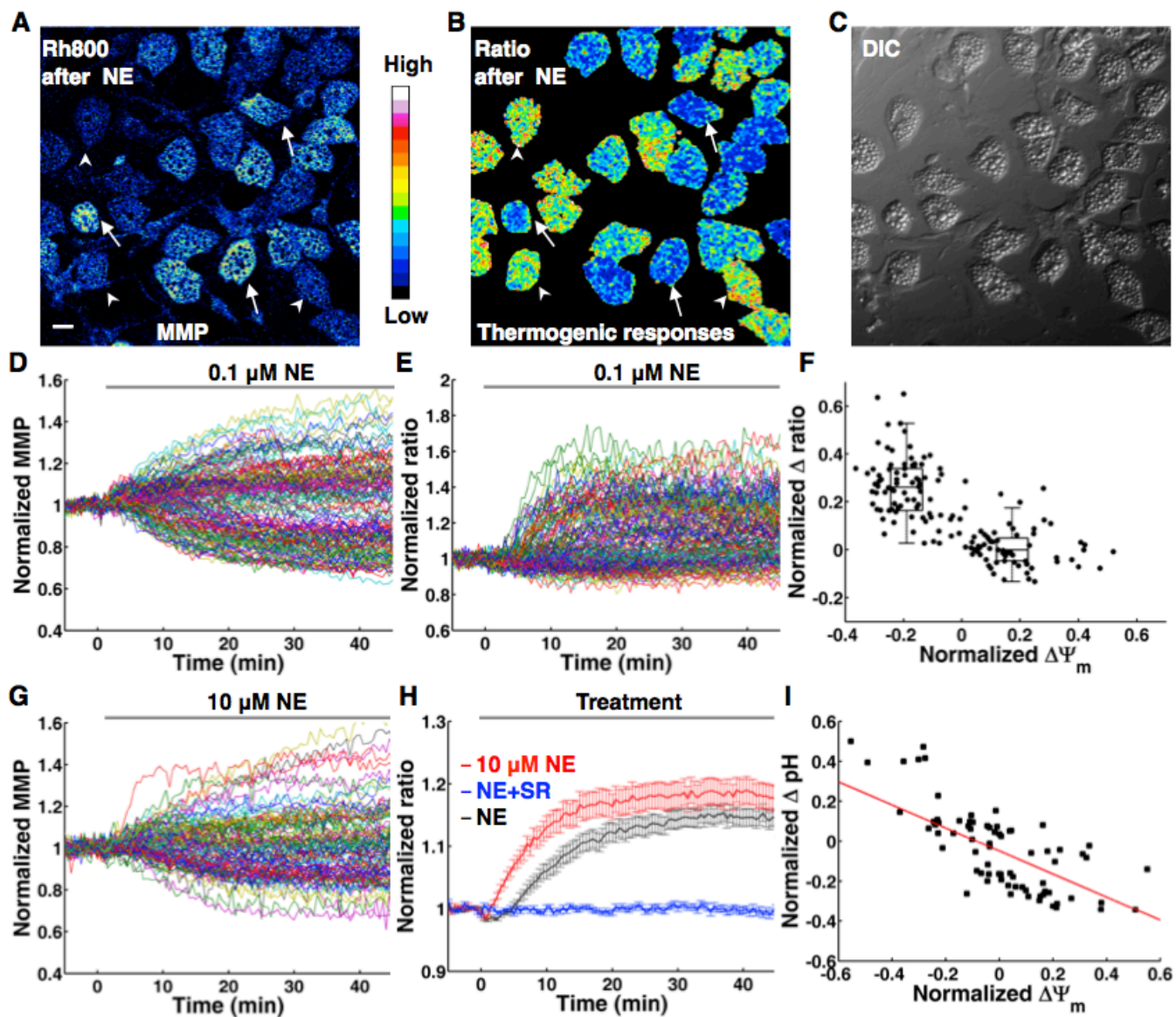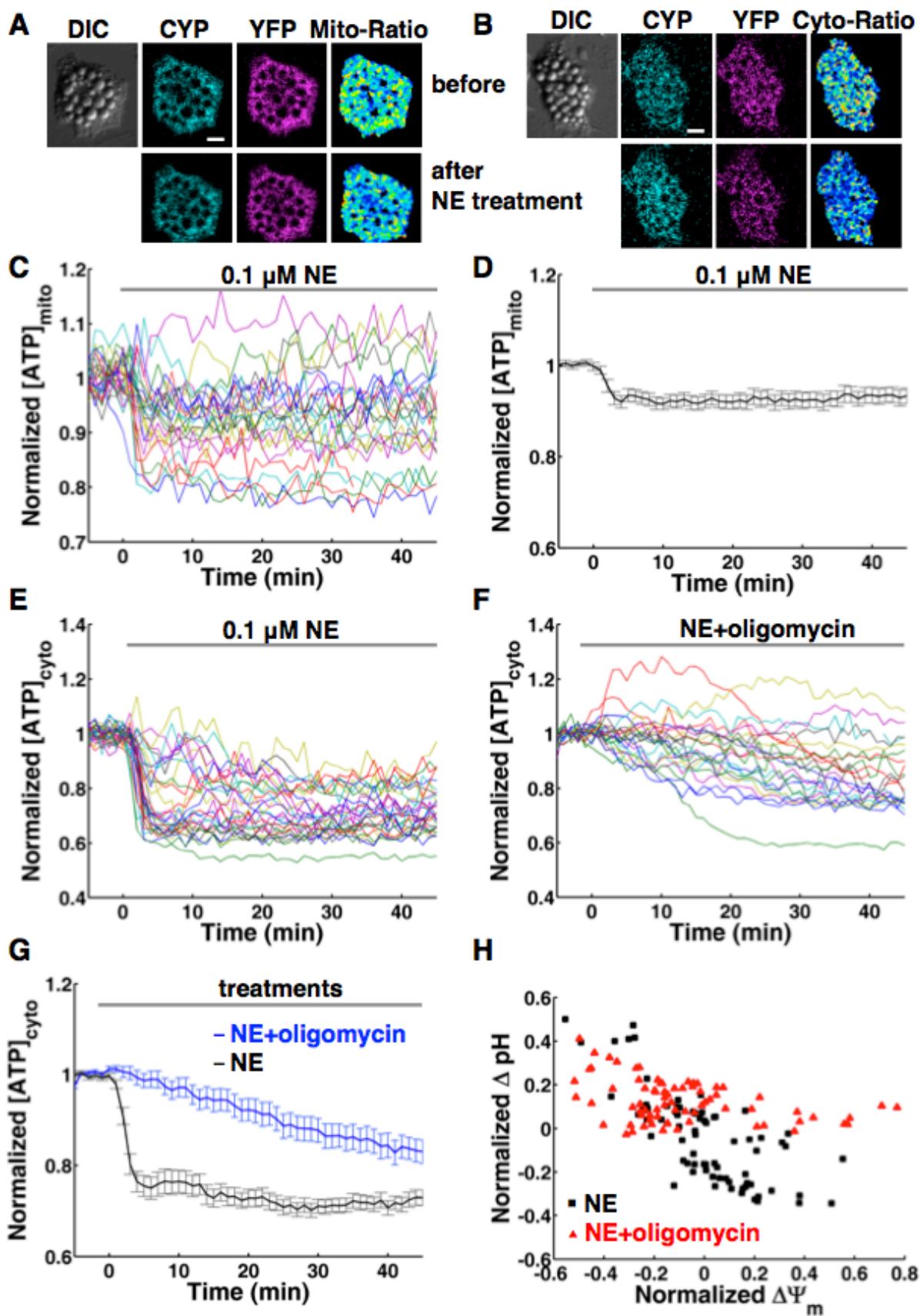
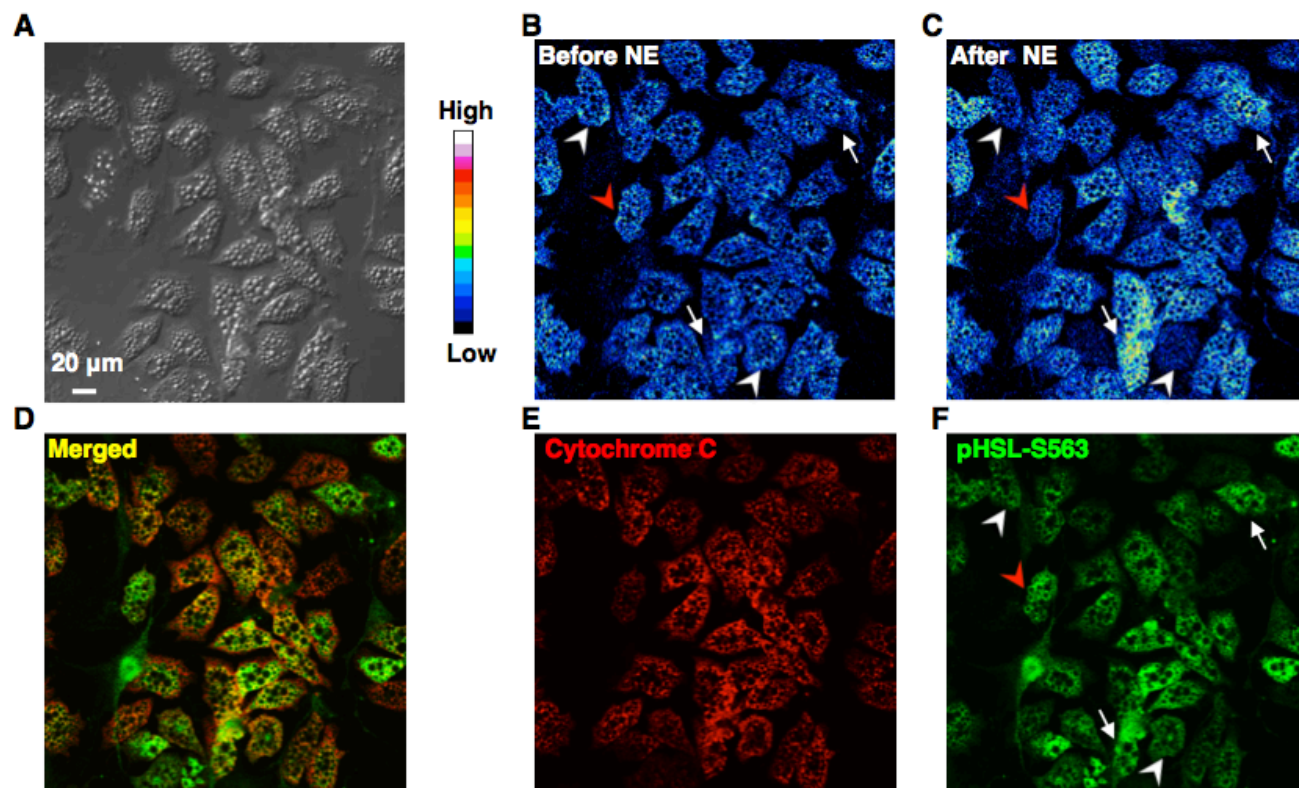**Figure 1**

1   **Figure 2**

Figure 3

1   **Supporting online material**

2

3   **1. Supplemental figures**

4

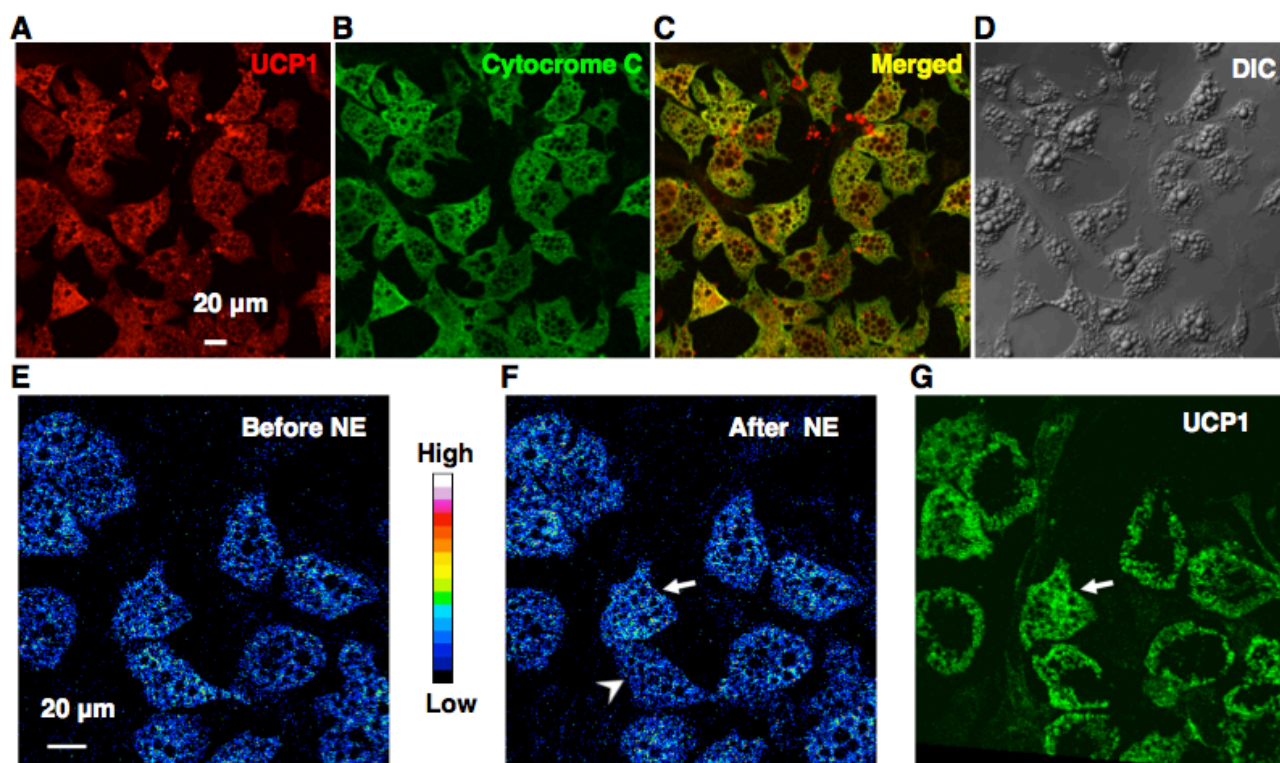5   **Figure S1**
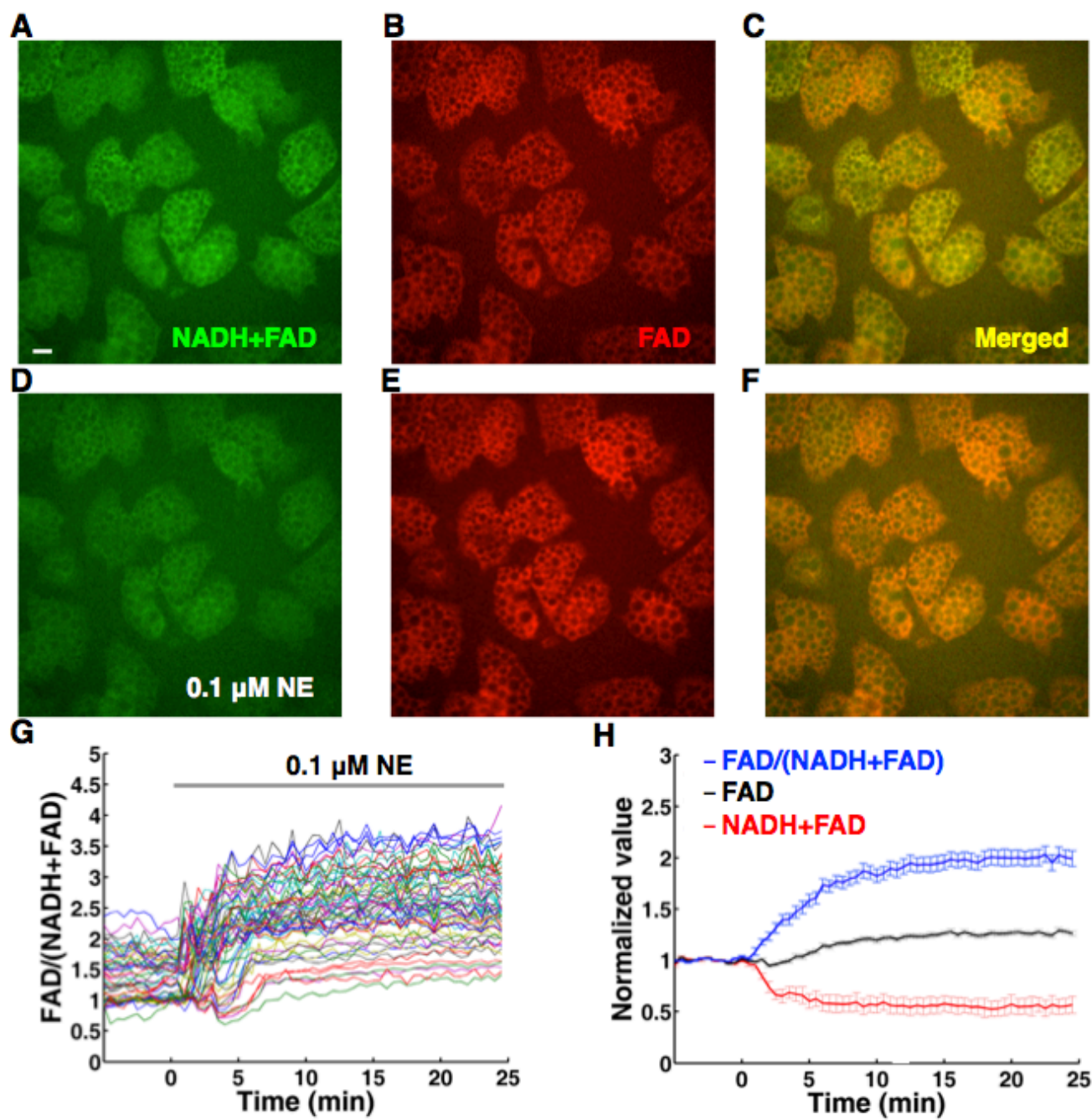
6

1

2

3 **Figure S2**
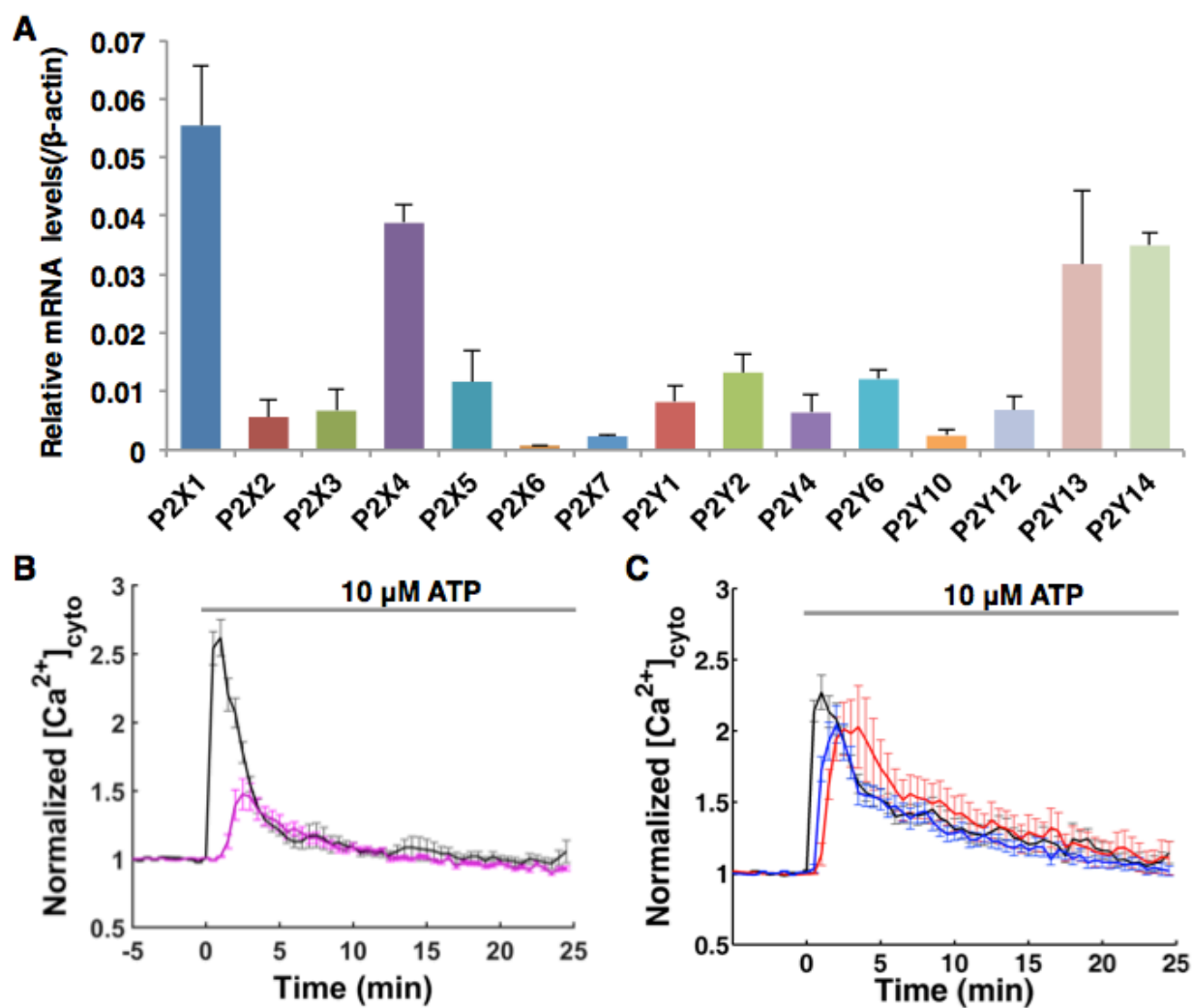
4

1

2

3   **Figure S3**

4

1

2

3   **Figure S4**

1 **2. Supplemental figure legends**

2

3 **Figure S1. NE-induced heterogeneous changes of mitochondrial membrane potentials (MMP) are not correlated to the**

4 **heterogeneity of phospho-HSL levels.** (**A-C**), Merged confocal images of mitochondria in BA stained with 20 nM

5 mitochondrial marker Rh800. Scale bar, 20 μm. (**A**), Differential interference contrast (DIC) image of multilocular BA. (**B** and

6 **C**), Representative images of mitochondrial membrane potential (represented with Rh800 intensity) are shown for the

7 moments before and after 0.1 μM NE treatment respectively. Arrow heads point to BA with mitochondrial depolarization,

8 while arrows point to BA with mitochondrial hyperpolarization. (**D-F**), Heterogeneous changes of MMP in BA are not

9 correlated with phosphorylated levels of HSL. Retrospectively immunostained images of BA after NE treatment. (**D**), Merged

10 image of BA stained with antibodies against cytochrome C (red, **E**) and phosphorylated HSL (green, **F**). Red arrow head

11 points to BA with mitochondrial depolarization (**B** and **C**) and high level of phosphorylated HSL (**F**), while white arrows point

12 to BA with mitochondrial hyperpolarization (**B** and **C**) and high level of phosphorylated HSL (**F**). Meanwhile, arrow heads

13 show BA with mitochondrial depolarization (**C**) and low level of phosphorylated HSL (**F**).

14

15 **Figure S2. Hyperpolarization of MMP in BA is not due to the absence or heterogeneity of UCP1 levels.** (**A-D**),

16 Confocal images of BA immunostained with antibodies against UCP1 (red, **A**) and Cytochrome C (green, **B**). Scale bar,

17 20 μm.   **C**, Merged image of immunostained BA. (**D**), Differential interference contrast (DIC) image of BA. (**E** and **F**),

18 Hyperpolarization of MMP in BA is not correlated with expression levels of UCP1. Representative images of

19 mitochondrial membrane potential (represented with Rh800 intensity) are shown for the moments before and after 0.1

20 μM NE treatment respectively. (**G**), Confocal images of BA retrospectively immunostained with antibody against UCP1

21 after NE treatment (**E** and **F**). Arrow points to BA with mitochondrial hyperpolarization with high level of UCP1, while

22 arrow head shows BA with mitochondrial depolarization.

23

24 **Figure S3. Redox ratio measurement for NE stimulation in BA.** (**A-H**), Autofluorescence of FAD and NADH based

25 redox ratio measurements. Scale bar, 20 μm. (**A** and **D**), show autofluorescence images of FAD + NADH signals before

26 and after 0.1 μM NE treatment respectively, while (**B** and **E**) show autofluorescence images of FAD before and after NE

27 treatment respectively. (**C** and **F**) are merged redox ratio images of FAD (red) to FAD+NADH (green). (**G**), The raw

28 data plots of redox ratio change in 0.1 μM NE treated BA. Each colored trace represents redox change of single BA (n =

29 60). (**H**) shows the normalized averaged FAD, FAD+NADH and redox change after NE treatment. All data points in (**H**)

30 represent mean ± SEM.

31

32 **Figure S4. Sympathetic cotransmitter ATP increases intracellular [Ca^{2+}] in BA through multiple P2 receptors.**

33 (**A**), The quantitative-PCR results show the expression levels of P2 receptors in BA, including P2X1, P2X2, P2X3,

34 P2X4, P2X5, P2X6, P2X7, P2Y1, P2Y2, P2Y4, P2Y6, P2Y10, P2Y12, P2Y13 and P2Y14. (**B** and **C**), show that ATP

35 induces cytoplasmic [Ca^{2+}] transient in BA can be dramatically decreased with multiple inhibitors of P2 receptors (**B**),

36 and less affected by single inhibitor of P2X receptor (**C**). (**B**) shows that the combination of multiple inhibitors (10 μM

37 PPADS, a nonselective inhibitor of P2X receptor; 2.5 μM PSB 0739, an antagonist of P2Y12; 0.5 μM MRS 2279, an

38 inhibitor of P2Y1; 100 μM Suramin, a nonselective inhibitor of P2Y receptor) can largely decrease the cytoplasmic

39 [Ca^{2+}] transient induced by ATP stimulation (Control, black, n = 25; multiple inhibitors, magenta, n = 21). (**C**) shows

40 that single inhibitor has little effect to reduce cytoplasmic [Ca^{2+}] transient induced by ATP stimulation (Control, black, n

41 = 17), such as a selective antagonist of P2X1 (10 μM PPNDS, blue, n = 14) or nonselective inhibitor of P2X receptor

42 (10 μM PPADS, red, n = 13). All data points in **A-C** represent mean ± SEM.

43

44

3. Supplemental Video Legends

Supplemental Video 1 | Subpopulations of NE-induced thermogenesis in BA. The ratiometric pseudocolor movie of 0.1 μM NE-induced thermal responses in BA. Scale bar, 20 μm.

Supplemental Video 2 | NE-induced heterogeneous responses in BA. The raw channel data of supplementary video 1 show BA subpopulations after NE treatment. Red represents the channel of thermosensitive RhB-ME, while green represents thermoneutrol Rh800. Scale bar, 20 μm.

Supplemental Video 3 | NE and ATP co-induced thermogenesis in BA. The ratiometric pseudocolor movie of co-treatment with 0.1 μM NE and 10 μM ATP-induced thermal responses in BA. Scale bar, 20 μm.

Supplemental Video 4 | Raw data of NE and ATP co-induced thermogenesis in BA. The raw channel data of supplementary video 3 show BA subpopulations after NE and ATP co-treatment. Red represents the channel of thermosensitive RhB-ME, while green represents thermoneutrol Rh800. Scale bar, 20 μm.

Supplemental Video 5 | ATP-induced cytoplasmic $[Ca^{2+}]$ transient in BA. The merged pseudocolor movie of 10 μM ATP-induced cytoplasmic $[Ca^{2+}]$ transient in BA. Scale bar, 20 μm.

4. Supplemental Materials

General materials

Rhodamine B (RhB), Rhodamine 800 (Rh800), and carbonyl cyanide m-chlorophenyl hydrazone (CCCP), rotenone, oligomycin A, adenosine triphosphate (ATP), anti-UCP1 (U6382, rabbit), collagenase type II, cytosine arabinoside (Ara-C), Ficoll 400, glutathione, glucose, Hepes, KCl, NaCl, $MgCl_2$ and $CaCl_2$ were purchased from Sigma-Aldrich Corporation (USA). Norepinephrine (NE) and Dimethyl Sulfoxide (DMSO) were purchased from Santa Cruz Biotechnology, Inc. (USA). SR-59230A was purchased from Abcam Inc. (UK). SNARF1-AM, Fura2-AM, Dulbecco's Modified Eagle Medium (DMEM), fetal bovine serum (FBS), newborn calf serum (NCS), ALEXA-488 goat anti-rabbit, ALEXA-555 goat anti-mouse, Phosphate-Buffered Salines, pH7.4 (PBS) and Penicillin Streptomycin (Pen Strep) were purchased from Thermo Fisher Scientific Co., Ltd. (USA). Anti-Phospho-HSL (Ser563, 4139, rabbit) was purchased from Cell Signaling Technology (USA). Matrigel and anti-cytocrome C (556432, mouse) were purchased from BD Biosciences Company (USA). Coverslips were purchased from Glaswarenfabrik Karl Hecht GmbH & Co KG (Germany).

C57BL/6J mice were purchased from Sino-British SIPPR/B&K Lab Animal Ltd., Shanghai (China). All experimental procedures and protocols were approved by the Institutional Animal Care and Use Committee of the Institute for Nutritional Sciences, Shanghai Institutes for Biological Sciences, Chinese Academy of Science.

All confocal imaging was performed using confocal microscope FV1000 (Olympus Corporation, Japan). The other fluorescence imagings were performed using a customized fluorescence microscope (BX61WI, Olympus Corporation, Japan) equipped with Optoscan monochromator (Cairn Research Ltd., UK), customized emission filters (Semrock, USA) and Evolve 512 EMCCD (Photometrics Ltd., USA), which were all controlled with customized Micro-Manager software.

Thermogenic study

All imagings were performed using confocal microscope with a 40×/0.95 objective (Olympus) for time-lapse imaging and a 100×/1.4O objective (Olympus) for high-resolution imaging. Cells were co-stained with RhB-ME and Rh800 (20 nM dyes for time-lapse imaging, 50 nM dyes for high resolution imaging) in Tyrode's solution (in mM: 10 Hepes, 10 glucose, 3 KCl, 145 NaCl, 1.2 $CaCl_2$, 1.2 $MgCl_2$, pH 7.4) for 1 h at 33 °C (10). The pseudocolor of RhB-ME channel is red (excited at 559 nm and collected at 575-620 nm), and Rh800 channel is green (excited at 635 nm and collected at 655-755 nm). All images were collected at 512 × 512 (for time-lapse imaging) and 1600 ×1600 (for high resolution imaging) pixels resolution (12 bit).

To minimize the heat influence by perfusion solution, time-lapse imaging of BA was performed in 2 mL Tyrode's solution rather than in perfusion system. To minimize bleaching and damage to live BA in time-lapse imaging, the lowest intensity of lasers with largest pinhole setting and the shortest scanning time were used, and 101 frames were recorded in a time-lapse imaging at 30 seconds interval. NE (0.1 μM), ATP (10 μM), or vehicle was injected as soon as the 11th frame of the time-lapse imaging for thermogenesis studies in BA. SR-59230A (1 μM), or oligomycin (10 μg/mL) was injected 15 min before the time-lapse imaging in pharmacological tests.

After background being removed, ratiometric values of Rh800 channel to RhB-ME channel (simultaneously excited by 635 nm and 559 nm lasers) were calculated pixel by pixel to represent the thermal response of the sample. For noise reduction, the pixels with signal-to-noise ratios less than 1.5 were excluded and 5×5 moving average was used before ratiometric process. According the three-sigma rule, the outlier (99.7% tolerance interval) of the ratios was also excluded. The ratio of each cell was the average ratio of all pixels representing the cell. Since we focus on the thermal responses, the mean ratio of steady state before drug treatments was used to normalize every data point for each cell. All data analysis was performed with MATLAB (MathWorks Inc. USA) and ImageJ (NIH, USA).

Primers for quantitative-PCR analysis of P2 receptors in BA

1   Total RNA of cultured brown adipocytes were extracted and prepared with Trizol (Thermo Fisher, Cat No: 15596-026).

2   First strand cDNAs were synthesised using oligo(dT)18 primers (Thermo Fisher, First Strand cDNA Synthesis Kit, Cat No:

3   K1612) and RT-PCR reagent, which contains 4.6 µl cDNA (100 ng/µl), 0.2 µl each primer (10 µM) and 5 µl SYBR green mix

4   (Thermo Fisher, Cat No: 4367659). The paired primers of *P2x* and *P2y* were listed as below:

5

	Forward primers	Reverse primers
Actin	5'-TTCTTTGCAGCTCCTTCG-3'	5'-TTCTGACCCATTCCCACC-3'
P2x1	5'-GACAAACCGTCGTCACCTCT-3'	5'-ATCCCAGAGCCGATGGTAGT-3'
P2x2	5'-CCACCACCACTCGAACTCTC-3'	5'-CAGAGCAGTGGCCAGATTGA-3'
P2x3	5'-TCCTGAAGGCTTTCGGCATC-3'	5'-CACTCCCACGGAAGTGAAGG-3'
P2x4	5'-CCCAGATATTCCTTCCGGCG-3'	5'-GTGAGTGTGCGTTGCTCATT-3'
P2x5	5'-GCCAGGTATTACCGTGACCC-3'	5'-CTGAATTTTCCCGCCTTGCC-3'
P2x6	5'-ACCCAGGTTAAGGAGCTGGA-3'	5'-TGGTGTCACGAGGAAGTTGG-3'
P2x7	5'-GGGGTGACGAAGTTAGGACA-3'	5'-ACTTGGCCTTCTGACTTGACA-3'
P2y1	5'-CCAATGTGCCCTGACCAAGA-3'	5'-ACATCCAGATAGCCACGCTG-3'
P2y2	5'-TCCTATGCCGCCTCAAAACC-3'	5'-TAAATGGCCAGTGGTCACCC-3'
P2y4	5'-CCAACCCTTTGGCTGTTCCT-3'	5'-GGGCAGTGACAGCACATACA-3'
P2y6	5'-GGGTAGTGTGTGGAGTCGTG-3'	5'-GCGAGTAGACAGGATGGGTG-3'
P2y10	5'-ACTGCCTGTTTGCCATTTCC-3'	5'-CAACCATGGTGACCAGAACCA-3'
P2y12	5'-GTTCCCTTCCACTTTGCACG-3'	5'-AGGGTGCTCTCCTTCACGTA-3'
P2y13	5'-CCGTCTGGTCCCTGATGTTC-3'	5'-GCCCAAGGGGACTCTTCAAA-3'
P2y14	5'-CCACATTGCCAGAATCCCCT-3'	5'-AGCCGAGAGTAGCAGAGTGA-3'

6

7   All the reagents were pipetted into 384-well plate, gently spun down, and placed in 7500 Real-Time PCR System (ABI).

8   Samples were Incubated at 95°C for 10 min, followed by 40 cycles of 95°C for 25 s, 60°C for 30 s, and 72°C for 30 s. Data

9   were collected and analyzed by being normalized with actin.